Segregation of Ba^{2+}, Sr^{2+}, Ce^{4+} and Zr^{4+} to UO_2 surfaces

2004 J. Phys.: Condens. Matter 16 S2699

(http://iopscience.iop.org/0953-8984/16/27/008)

INSTITUTE OF PHYSICS PUBLISHING JOURNAL OF PHYSICS: CONDENSED MATTER

J. Phys.: Condens. Matter **16** (2004) S2699–S2714 PII: S0953-8984(04)72316-4

Segregation of Ba^{2+}, Sr^{2+}, Ce^{4+} and Zr^{4+} to UO_2 surfaces

C R Stanek[1,2], M R Bradford[3] and R W Grimes[2]

[1] Division of Materials Science and Technology, MS-G755, Los Alamos National Laboratory, Los Alamos, NM 87545, USA
[2] Department of Materials, Imperial College, London SW7 2BP, UK
[3] British Energy Generation Ltd, Barnwood, Gloucestershire GL4 3RS, UK

E-mail: r.grimes@imperial.ac.uk

Received 20 November 2003, in final form 4 January 2004
Published 25 June 2004
Online at stacks.iop.org/JPhysCM/16/S2699
doi:10.1088/0953-8984/16/27/008

Abstract

Segregation of the cation substitution defects Ba^{2+}, Sr^{2+}, Ce^{4+} and Zr^{4+} to the stable low index surfaces of UO_2 has been predicted using atomistic simulation techniques. While Ce^{4+} and Zr^{4+} substitute simply for U^{4+}, charge compensation in the form of oxygen vacancies is required in the case of Ba^{2+} and Sr^{2+}. Three surfaces are considered: (110), (111) and (100). Although the (111) and (110) are perfect cleaved surfaces, the (100) necessarily incorporates a series of surface defects to neutralize the inherent dipole. The segregation energies of these cations depend strongly on the surface to which the segregation is proceeding. Furthermore, it is also a function of the orientation of the segregating defect cluster with respect to the surface and, in the case of the (100) dipolar surface, the configuration of the surface defects.

(Some figures in this article are in colour only in the electronic version)

1. Introduction

Theoretical explanations for surface segregation date back to Gibbs in the 19th century [1], and his description of a *dividing surface* between two bulk phases. Despite such a long history of qualitative understanding, it is only recently that analytical instruments have been developed with sufficient resolution to investigate this phenomenon at the atomic level. However, segregation trends remain difficult to extract from experimental data. This can be attributed to the complexity of segregation processes, which are influenced by such issues as compensating charged surface defects and interactions between segregating species at and beneath the surface. As a result, atomistic simulation techniques are particularly useful in supplementing or helping to focus experimental effort.

This paper describes the results of an atomistic simulation study of the segregation of the substitutional ions Ba^{2+}, Sr^{2+}, Ce^{4+} and Zr^{4+} to the stable, low index surfaces of UO_2. It is important to note that substantial concentrations of Zr^{4+}, Ce^{4+}, Ba^{2+} and Sr^{2+} (in that order) are formed as fission products in irradiated UO_2 nuclear fuel [2, 3].

2. Previous work

2.1. Experimental segregation studies

In recent times, the seminal work of McCune and Wynblatt [4] has served as an impetus to motivate further work. They investigated the segregation of Ca^{2+} to the (100) surface of the prototypical ionic ceramic MgO, by using low energy ion scattering spectroscopy and Auger spectroscopy to measure equilibrium surface coverage. Roshko and Kingery similarly looked at segregation of Ca^{2+} in MgO [5], although they investigated three high angle grain boundaries using scanning transmission electron microscopy. Their results identified different segregation behaviours for Ca^{2+} to the different boundaries, indicating that grain boundary structure does have an effect on segregation.

In order to better understand the phenomenon whereby MgO beneficially affects the sintering of Al_2O_3, Baik and co-workers investigated the segregation of Mg^{2+} and Ca^{2+} to Al_2O_3 surfaces [6–8]. This work was partially motivated by a previous study [9] which suggested that even at low bulk concentrations of Ca^{2+} (5–15 ppm), there is pronounced Ca^{2+} segregation. Interestingly, Baik and co-workers found that for both Ca^{2+} and Mg^{2+}, the extent of segregation to the $(10\bar{1}0)$ prismatic plane was different to that to the (0001) basal plane [6–8].

2.2. Modelling segregation studies

The simulation of segregation to UO_2 surfaces was pioneered at the Theoretical Physics Division of Harwell Laboratory as part of an overall policy to develop general purpose atomistic simulation codes. The treatment of defect energies based on the two-region approach described by Lidiard and Norgett [10] led to the calculation of defect formation, clustering, migration and solution energies in UO_2 [3, 11–13]. These types of calculation have made a significant contribution to the understanding of fuel performance.

Building on previous work, our motivation in this case is to question one of the assumptions of the Booth model: that the release of fission products from a grain of UO_2 is isotropic (see [14] and references therein). If segregation can be shown to be surface dependent, there is an implication that release will show a degree of anisotropy. This may have significance for the development of future fuel performance codes.

Despite the potential importance, there have been relatively few simulation studies of segregation as compared to equivalent studies of bulk materials or even surface structure. Perhaps the earliest simulation studies were those of Tasker *et al* [15–18], who used pair potential calculations to determine surface energetics and segregation trends in metal oxides. In particular, they combined detailed atomistic simulation techniques with simple statistical mechanics to describe Ca segregation to surfaces of MgO [15]. The results obtained were in agreement with the experimental results of McCune and Wynblatt highlighted above [4]. Defect formation energies near surfaces and grain boundaries were also investigated [16, 17]. In these studies, it was found that defect formation energies varied with depth from the surface or boundary. This result suggested that the population and kinetics of defects are surface or boundary type dependent. Tasker *et al* then expanded the scope of their work by considering the segregation of an extensive range of divalent cations to (001) and (110) surfaces of MgO and CaO [18]. From this, they were able to predict that Fe^{2+}, Mn^{2+}, Ca^{2+}, Ba^{2+} and Sr^{2+} will

segregate to the (001) surface of MgO. An interesting review of these studies can be found in a paper by Tasker and Mackrodt [19].

With a method well established to determine segregation trends to surfaces of simple oxides, more complex materials were duly investigated. Davies *et al* [20] studied the segregation of various dopants to surfaces of oxides with the corundum structure. The results for Ca segregation to the prismatic plane of Al_2O_3 qualitatively agreed with the experimental results of Baik *et al* [7], though they noted that the results for the basal plane were not as convincing. Nevertheless, importantly they found segregation enthalpy to be coverage dependent in contrast to the Langmuir adsorption model.

A paper by the same group reported improved simulation results for impurity segregation to surfaces of Al_2O_3 [21], confirmed by comparison of their results for Mg and Ca segregation in Al_2O_3 to the experimental work of Baik *et al* [7] and Mukhopadhyay *et al* [6]. They then described the segregation of Ca to (111) and (110) surfaces of ZrO_2. In this paper [21], morphology as well as the generation of segregation paths via molecular dynamics were discussed. Similar techniques have been used more recently, as reported in a paper by Cooke and Parker [22], who investigated the segregation of isovalent impurities to the (001) and (021) surfaces of haematite. This group has also considered perfect and defective surfaces of Cr_2O_3 [23].

Of particular relevance to the work in this paper is the study by Sayle *et al* [24], which investigated the segregation of Rh^{3+}, Pd^{2+} and Pt^{2+} to the (111) and (110) surfaces of CeO_2. For Pd^{2+} and Pt^{2+}, they found preferential segregation of isolated defects as well as the formation of coherent second phases only at the (111) surface.

More recently, Slater *et al* [25] investigated the segregation of Sb and associated oxygen vacancies to the (110) and (001) surfaces of SnO_2. Segregation energies were calculated by comparing the energy for each defect complex in the bulk and on the surface.

In an attempt to improve upon previous Langmuir–McLean type approaches [15, 18, 19, 26], LeSar *et al* [27] developed a free energy minimization technique that uses the interionic pair potential approach to calculate not only enthalpy, but also changes in vibrational entropy via a local harmonic lattice dynamics approximation. Furthermore, they were able to consider changes in solute concentration by using a mean-field effective atom representation [28]. This technique was used by Battaile *et al* [29] to calculate the segregation of isovalent solute cations in cubic oxides. These results were compared to those obtained using the conventional Langmuir–McLean method. The two methods were found to agree well, which suggested to Battaile *et al* [29] that vibrational effects are of only secondary importance in determining the segregation to free surfaces, this was also concluded by Davies *et al* [20]. However, Battaile *et al* [29] noted that the Langmuir–McLean method fails to reproduce subsurface segregation, which they found to be an important phenomenon.

3. Surfaces of UO_2

The three stable, lowest index surfaces of UO_2, as defined by Miller indices, are (110), (111) and (100). Following the classification of Tasker [30], the (110) surface is a neutral type 1 surface and therefore has no surface normal dipole to account for. The anion terminated (111) surface has charged individual planes although there is no dipole perpendicular to the surface (so long as the block is cut at the appropriate layer) and is therefore denoted as type 2. The (100) surface is of the unstable type 3 distinction. In order to create a physically stable (100) surface, a series of vacancies must be formed on the surface. In the case of cation terminated UO_2, half an oxygen layer is moved from the bottom of the simulated bulk to the surface and this serves to neutralize the dipole. The neutralizing oxygen ions can be configured in many different ways.

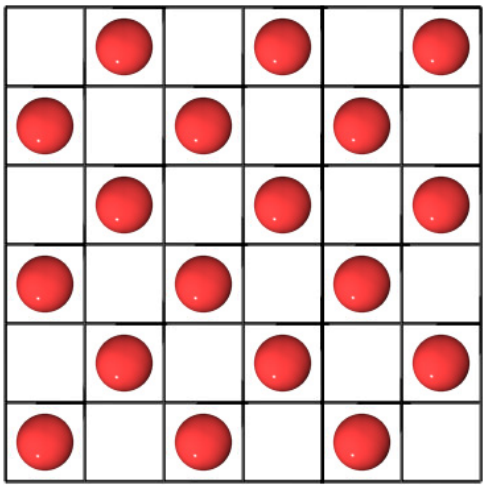

Figure 1. The anion termination of the 3 × 3 unit cell (100) UO_2 surface considered in this work, calculated to be low energy by Abramowski [31].

For example, Abramowski calculated the surface energies for the 153 unique configurations of a surface layer 2 × 2 unit cells in size [31]. Of these 153 configurations, Abramowski found that several exhibited low surface energies, but of these one had an attachment energy much closer to zero (and therefore will be more in evidence; see [32] for more details of surface and attachment energies). Consequently, we will investigate only this one stable slow growing configuration where the configuration ions are diagonally opposing (see figure 1). Nevertheless, it is noted that consideration of other low energy configurations is worthwhile and this is discussed further elsewhere [33].

4. Methodology

4.1. Simulation techniques

Since these calculations are not based on a dynamic approach, it is necessary to develop a strategy to determine segregation trends from available data (the cations would in any case move only very slowly on a molecular dynamics timescale). Here, the simulations are based upon repeating a characteristic block of lattice with finite thickness in two dimensions. This block is then divided into region I and region II, in a similar manner to that used in bulk defect calculations [10, 34] (in these calculations, region I extends down approximately 18 Å and region II extends to a total of 85 Å). Thus all ions in region I are relaxed explicitly, but ions in region II are held fixed and are included only to approximate the effect on region I ions of the remaining perfect bulk crystal. A defect is then placed at a lattice site towards the bottom of region I, which is assumed to represent the interior or a bulk lattice site. The defect is then systematically moved stepwise to the surface, with an energy minimization calculation being performed at each layer. The total energies of the repeat units with the segregating defects in different positions can then be compared to one another and a plot of energy as a function of depth constructed. By means of relative energies, this approximately describes the chemical potential, which is the driving force for segregation.

Of concern here, and indeed with any atomistic calculation, is the size of the repeated simulation cell. Initially this work began using a simulation cell of 1 × 1 × 6 unit cells

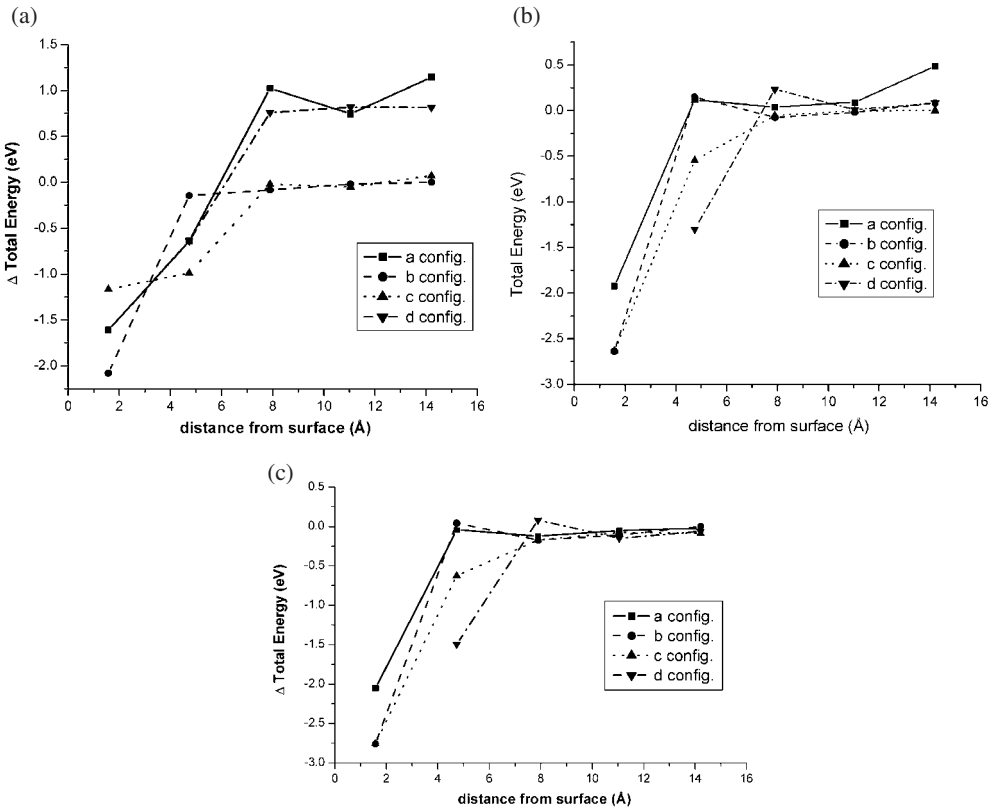

Figure 2. Relative energies of the cluster $\{(Ba_U)'':(V_O)^{\cdot\cdot}\}^x$ calculated as a function of depth from the (111) surface using (a) $1 \times 1 \times 6$, (b) $2 \times 2 \times 6$ and (c) $3 \times 3 \times 9$ simulation cells. As the simulation cell increases in size, unphysical defect–defect interactions are reduced.

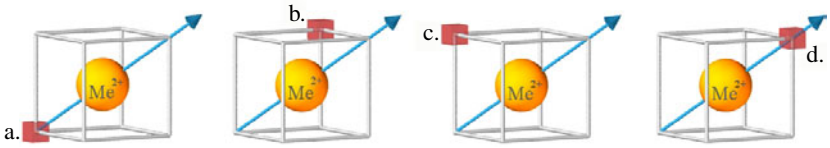

Figure 3. The four unique $\{(Me_U)'':(V_O)^{\cdot\cdot}\}$ cluster configurations with respect to the (111) surface, where the arrow indicates the direction of that surface (i.e. the surface normal). The notation for the cluster configurations is maintained throughout the text.

in size (i.e. 71 ions). Unfortunately, this was far too small, and gave rise to unphysical defect–defect interactions perpendicular to the surface (i.e. between repeat units). This defect–defect interaction is evident in figure 2(a), which depicts the segregation trends for the $\{(Ba_U)'':(V_O)^{\cdot\cdot}\}^x$ cluster. In this plot, there is a pronounced energy gap between the sets of data labelled (a) and (d) configuration, and the sets of data labelled (b) and (c) configuration (where (a), (b), (c) and (d) correspond to the different oxygen vacancy positions; see figure 3). Critically, this difference does not diminish as a function of increasing distance from the surface.

To reduce the defect–defect interactions, larger simulation cells are necessary. For the $2\times2\times6$ simulation cell (i.e. 287 ions) shown in figure 2(b) the four configurations are somewhat closer in energy at a depth of 12 Å from the surface but a split between configuration a and

Table 1. Short range pair potential parameters; see equation (1).

Species	A (eV)	ρ (Å)	C (eV Å^6)	Reference
O^{2-}–O^{2-}	9547.96	0.2192	32.0	[43]
Zr^{4+}–O^{2-}	1502.11	0.3477	5.10	[44]
Ce^{4+}–O^{2-}	1809.68	0.3547	20.40	[45]
U^{4+}–O^{2-}	1761.78	0.3582	12.3	
Ba^{2+}–O^{2-}	905.70	0.3976	0.0	[46]
Sr^{2+}–O^{2-}	682.17	0.3945	0.0	[47]

Table 2. Shell model parameters.

Species	Y (e)	k (eV Å^{-2})	Reference
O^{2-}	−2.04	6.3	[43]
U^{4+}	−0.10	160.0	[48]
Zr^{4+}	−0.05	189.7	[44]
Ce^{4+}	−0.20	177.84	[44]

the other three occurs at 14 Å. This latter problem is because in configuration a, the vacant oxygen site is oriented towards the region I–region II interface. Thus it is necessary to increase the depth of region I. Therefore, a $3 \times 3 \times 9$ (i.e. 971 ions) unit cell simulation block was employed; see figure 2(c). It is clear from figure 2(c) that, using this large repeat cell, the total defect energies have converged sufficiently with respect to cell size to enable meaningful conclusions to be drawn from the calculations. The results which follow are denoted with the simulation cell size that was used.

4.2. Interaction between ions

The atomistic simulations described here were based upon a Born-like description of the lattice [35], using Buckingham potentials [36] to describe the short range interaction between ions. The lattice energy is therefore

$$E_{\text{lattice}} = \frac{1}{2}\sum_{i}\sum_{j\neq i}\left[\frac{q_i q_j}{4\pi\epsilon_0 r_{ij}} + A_{ij}\exp\left(-\frac{r_{ij}}{\rho_{ij}}\right) - \frac{C_{ij}}{r_{ij}^6}\right] \tag{1}$$

where q is the charge of the ion, ϵ_0 is the permittivity of free space, r_{ij} is the interionic separation and A_{ij}, ρ_{ij} and C_{ij} are the adjustable potential parameters for each pair of ions i, j. Table 1 lists the potentials used in this work and their origins. The polarizability of ions is accounted for by the shell model [37]. All ions except Ba^{2+} and Sr^{2+} are considered as polarizable, and their shell parameters are reported in table 2. The computational code CASCADE [38] was used to determine bulk perfect lattice energies, which were subsequently incorporated into MARVIN [39] which simulates surfaces and interfaces. The energies calculated by the different codes are comparable, as the same short range potential is used, and both codes rely on energy minimization techniques.

4.3. Solution sites

In this work, two types of segregating species are investigated, categorized by their charge state. Ce^{4+} and Zr^{4+} are isovalent with respect to U^{4+}, and therefore form simple substitutional defects (see [3] for details). Ba^{2+} and Sr^{2+} also substitute for uranium, but the dissimilar charge needs to be compensated by an oxygen vacancy. In common with all ceramic systems which contain

charged defects, for our case there is a strong attraction between the divalent substitutional ions and the oxygen vacancies. In the resulting neutral defect cluster $\{(Ba/Sr_U)'':(V_O)^{\cdot\cdot}\}^x$ the divalent metal ion is located essentially at the uranium site, but is displaced towards the oxygen vacancy which is located at a nearest neighbour site.

A complication arises with the $\{(Ba/Sr_U)'':(V_O)^{\cdot\cdot}\}^x$ defect cluster. In the bulk of UO_2, all nearest neighbour configurations of this defect cluster are equivalent. However, as the defect cluster nears the surface, this equivalence (i.e. symmetry) is broken. In different configurations, the distance of the oxygen vacancy from the surface varies. Consequently, the corresponding energies for each configuration may be different, and as a result each needs to be simulated. In fact, some symmetry remains so, with respect to the (111) surface, there are four unique configurations ((a)–(d); see figure 3), for the (110) surface there are three configurations ((a)–(c)) and for the (100) surface there are four configurations ((a)–(d)). Further discussion of this topic and corresponding diagrams depicting the configuration of each of these defect clusters with respect to each surface have been reported in a previous paper [40].

5. Results

5.1. The (111) surface

The segregation energy, E_S, is the difference between the internal energy of a fission product in the bulk and at the surface. It is therefore possible to compare *relative* energies which drive segregation trends. Results of Ce^{4+} and Zr^{4+} segregation to the (111) surface are shown in figure 4. Here, and throughout the paper, the depth from the surface corresponds to the unrelaxed z coordinate of the cation. Clearly, there is an energy penalty for segregation (i.e. a barrier) indicated by positive segregation energies: 0.232 and 0.261 eV for Ce^{4+} and Zr^{4+}.

Comparison of segregation trends is also facilitated by a second energy, E_T, which is defined as the difference between the energy of the fission product at the surface and the energy of the fission product in its most stable position, sometimes just beneath the surface, i.e. when $E_T > E_S$. In this regard, Zr^{4+} behaves slightly differently to Ce^{4+}. For Zr^{4+}, $E_T^{Zr} = 0.352$ eV, which is considerably greater than E_S, suggesting that although Zr^{4+} will not segregate to the (111) surface, it will become weakly trapped just below the surface. This trap is not evident for Ce^{4+}, with $E_T^{Ce}–E_S^{Ce} = 0.004$ eV. It is likely that the disparity in ionic radii between U^{4+} and Zr^{4+} (0.89 versus 0.72 Å respectively [41]) gives rise to the subsurface trapping phenomenon, while the similarity in ionic radius between U^{4+} and Ce^{4+} (0.89 versus 0.87 Å respectively [41]) explains the lack of trapping.

It should be noted that the methodology described above is very similar to that employed by Slater *et al* [25] as discussed in section 2.2. In their work, Slater *et al* define E_S as the difference between the energy of a defect in the bulk and at the surface, as it is here. However, the method used here (i.e. performing a calculation at each atomic layer, from the surface to the bulk) is more complete than that of comparing only the energy of a surface defect with that of a bulk defect. As elucidated by Battaile *et al* [29], subsurface segregation may be appreciable. Therefore, this methodological improvement accounts for previous limitations. (Nevertheless, our approach still only considers part of the complete segregation picture as kinetic barriers to migration of fission products to surfaces are not accounted for.)

From figures 2(c) and 5, it is clear that there is a pronounced driving force for both Ba^{2+} and Sr^{2+} to segregate to the (111) surface of UO_2 (with no subsurface trap). The segregation energies for Ba^{2+} and Sr^{2+} are $E_S^{Ba} = -2.706$ eV and $E_S^{Sr} = -1.603$ eV respectively. Clearly, the driving force for Ba^{2+} to segregate is greater than for Sr^{2+}. Again, this disparity in E_S can be attributed to ionic radius mismatch. The ionic radius for Sr^{2+} (1.18 Å) is more similar to U^{4+} (0.89 Å) than is the radius for Ba^{2+} (1.35 Å).

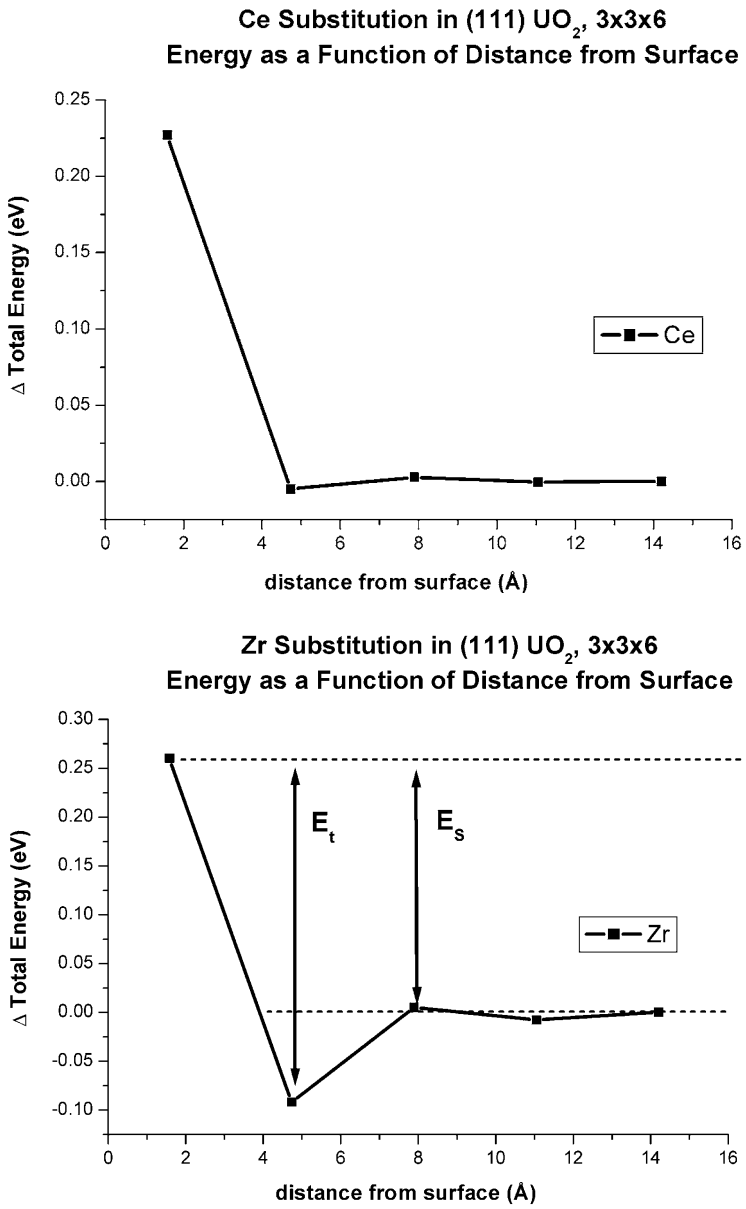

Figure 4. The calculated energies (relative to the energy in the bulk) of $(Ce_U/Zr_U)^x$ as a function of depth from the (111) surface, where E_T is the trap energy and E_S is the segregation energy.

Figures 2(c) and 5 also show that for these divalent cations, the bulk effectively begins 11 Å from the surface. Nearer to the surface, it appears that there is a cluster configuration dependence. This behaviour is a consequence of how the strain field induced by the cluster interacts with the strain field induced by the surface (i.e. a competition between the two ionic relaxation modes, one associated with the defect cluster and the other associated with the two-dimensional surface). For the isovalent cations Ce^{4+} and Zr^{4+}, the bulk effectively began only 8 Å from this surface.

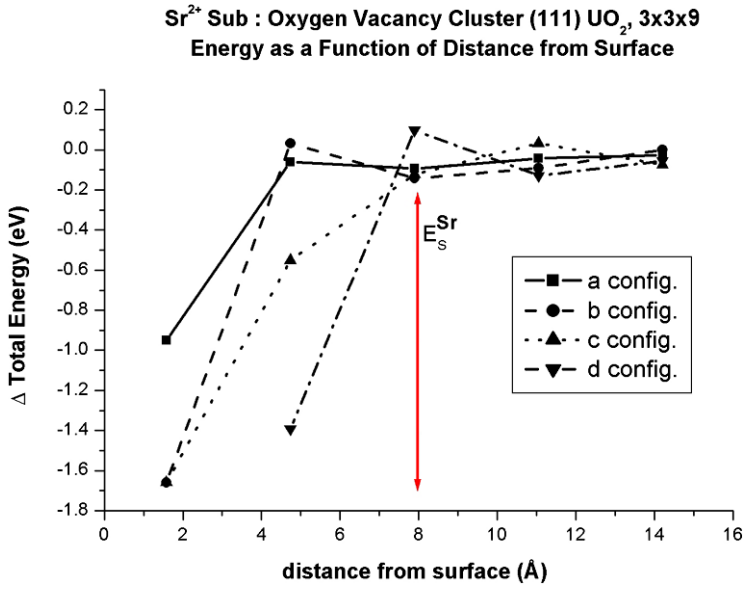

Figure 5. The calculated relative energies of the $\{(Sr_U)'':(V_O)^{\cdot\cdot}\}^x$ defect cluster as a function of depth from the (111) surface, where E_S is the segregation energy.

5.2. The (110) surface

There are clear similarities between the two plots in figure 6 and those in figure 4. The most obvious consequence of this is that Ce^{4+} and Zr^{4+} are predicted not to segregate to the (110) surface, as was the case with the (111) surface. However, upon closer inspection, it is clear that the segregation energy barrier for Ce^{2+} (0.67 eV) is greater than that of Zr^{4+} (0.13 eV). If these energies are compared to those obtained for the (111) surface (i.e. 0.232 and 0.261 eV for Ce^{4+} and Zr^{4+} respectively) the difference between Ce^{4+} and Zr^{4+} (110) is striking. Thus, the segregation barrier for Ce^{4+} is 0.435 eV larger for the (110) than for the (111) surface, while the segregation barrier for Zr^{4+} is 0.099 eV smaller. It is also apparent that the energy of Ce^{4+} within the bulk appears to vary more smoothly than Zr^{4+} (although the effect is exaggerated in figure 6 by the different y axis energy scales). This can again be attributed to the similarity in size between Ce^{4+} and U^{4+}, compared to U^{4+}. Consequently, the alternate compression and dilation of atomic layers which characterizes the (110) surface of the fluorite structure [31] has a greater effect on the relative energies of Zr^{4+} than on Ce^{4+}. Similar oscillations of isovalent solute concentration were observed by Battaile *et al* [29]. The dip in energy for Zr^{4+} at 6 Å means that as with the (111) surface, Zr^{4+} is trapped beneath the surface, although this trap is very weak indeed ($\approx$0.02 eV).

Figure 7 presents the results for Ba^{2+} and Sr^{2+} segregation to the (110) surface. It is clear that both ions tend to segregate to this surface, as was the case for the (111) surface. Also evident in figure 7 is that E_S^{Ba} is considerably more negative than E_S^{Sr}, suggesting a stronger tendency for Ba^{2+} to segregate than Sr^{2+}, which is again the same as for the (111) surface.

Two further interesting comparisons can be made between the energies of segregation of these divalent species to the (110) and (111) surfaces. First, the energies of segregation, E_S, for both Ba^{2+} and Sr^{2+} to these two surfaces are very similar: $E_S^{Ba} = -2.695$ eV for the (110) and $= -2.706$ eV for the (111); $E_S^{Sr} = -1.604$ eV for the (110) and $= -1.603$ eV for the (111). Second, the decrease in energy (and thus the driving force for segregation) begins

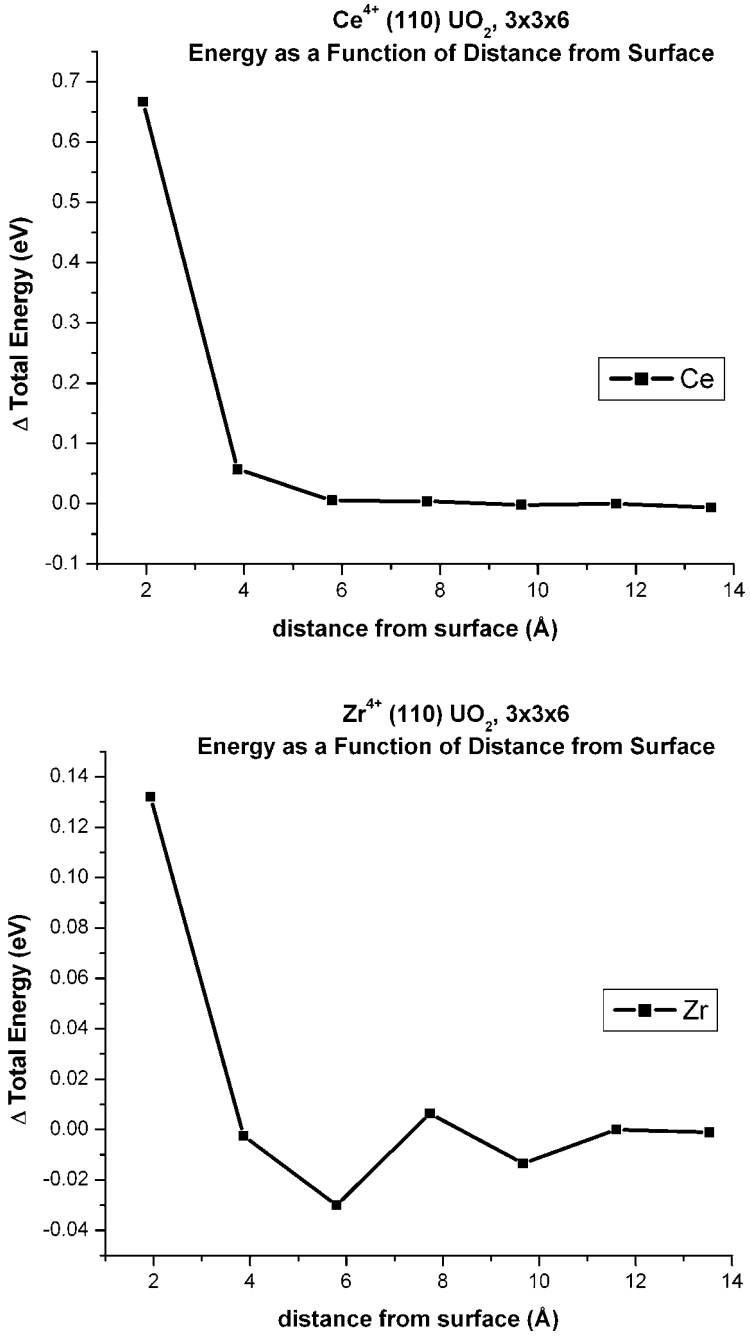

Figure 6. The calculated relative energies of $(Ce_U/Zr_U)^x$ as a function of depth from the (110) surface.

approximately 8 Å from the (110) surface (i.e. 3–4 layers), but only 5 Å from the (111) surface (i.e. 2 layers). Consequently, a greater concentration of Ba^{2+} or Sr^{2+} should build up adjacent to the (110) surface as compared to that adjacent to the (111) surface, despite the similarity in segregation energies, E_S.

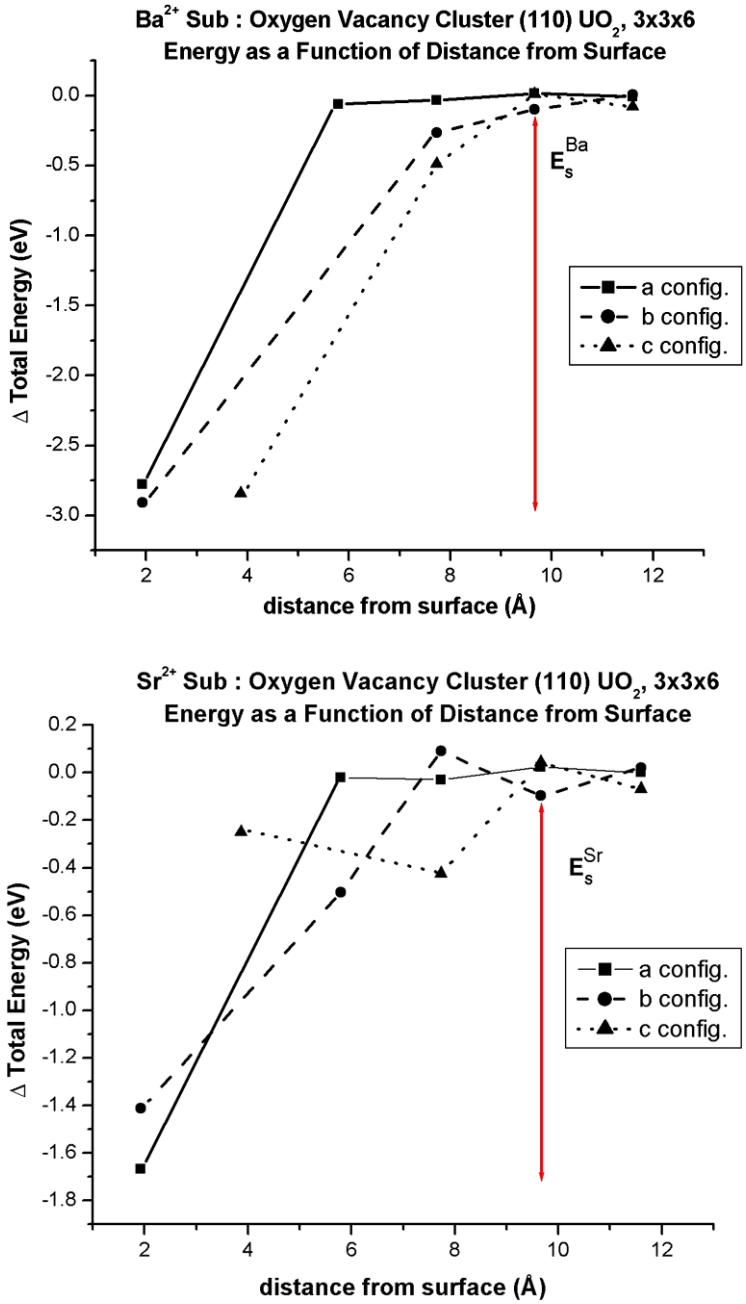

Figure 7. The calculated relative energies of the $\{(Ba_U/Sr_U)'':(V_O)^{\cdot\cdot}\}^x$ defect cluster as a function of depth from the (110) surface, where E_S is the segregation energy.

5.3. The (100) surface

Figure 8 depicts the results for Ce^{4+} and Zr^{4+} segregation to the (100) surface, with the half-layer of surface anions configured as described previously. For this dipolar surface, $E_S^{Ce} = -0.1221$

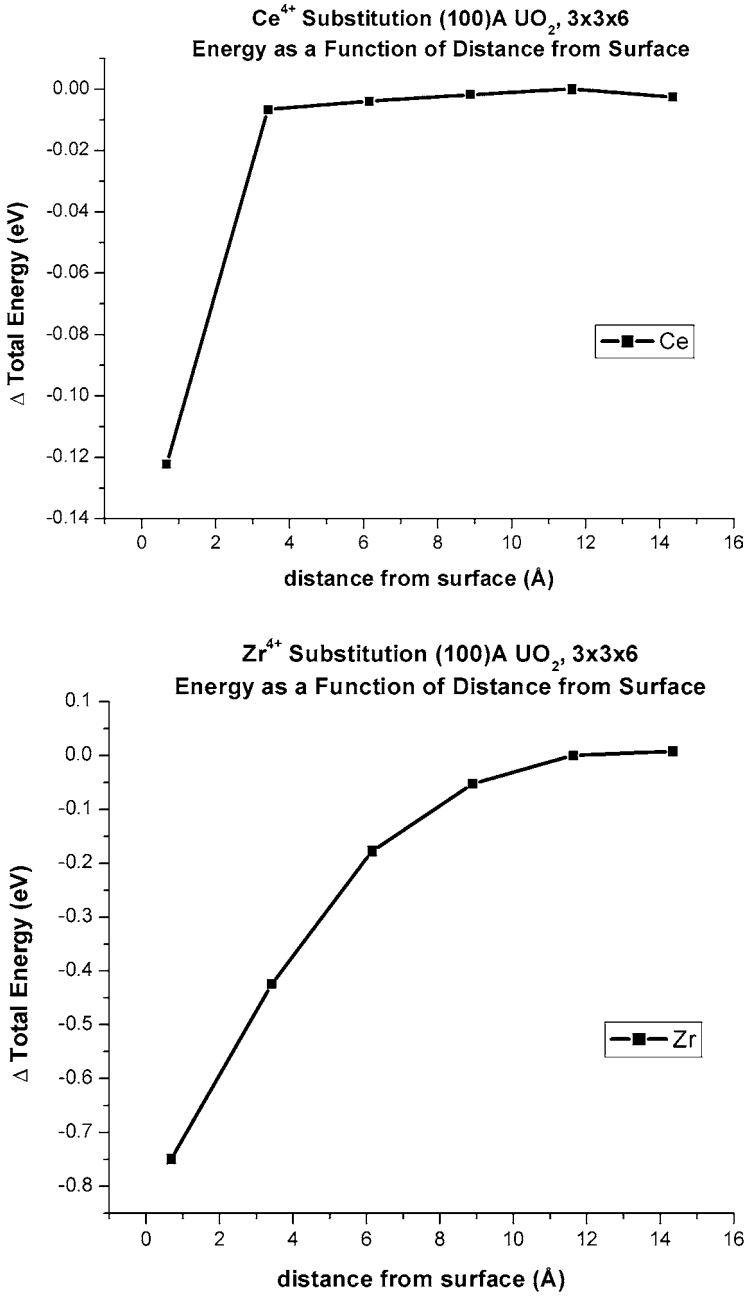

Figure 8. The calculated relative energies of $(Ce_U/Zr_U)^x$ as a function of depth from the (100) surface.

and $E_S^{Zr} = -0.7495$ eV. What is immediately striking about these values is that they are negative as opposed to the positive E_S values predicted for the other two low index surfaces (compare figures 8–4 and 6). Thus both Ce^{4+} and Zr^{4+} will segregate to the (100) surface, the opposite prediction to that for the (111) and (110).

Table 3. Summary of segregation energies.

	Segregation energy (eV)		
Cation	(111)	(110)	(100)
Ce^{4+}	0.23	0.67	−0.10
Zr^{4+}	0.25	0.13	−0.74
Ba^{2+}	−2.71	−2.7	−4.85
Sr^{2+}	−1.50	−1.60	−3.28

Figure 9 shows the results for Ba^{2+} and Sr^{2+} segregation to the (100) surface. Immediately, when comparing figure 9 with figures 5 and 7, clear differences are apparent. Although the segregation energies for Ba^{2+} and Sr^{2+} are again negative ($E_S^{Ba} = -4.8527$ and $E_S^{Sr} = -3.2844$ eV), with the result that these fission products will segregate to this surface, the profile of the energy from the bulk to the surface is different to that observed for the previous two surfaces. In both plots in figure 9, the '(c)' cluster configuration steadily decreases in energy as it moves to the surface, while the other three configurations decrease in energy abruptly near the surface. Also, in both cases, the '(a)' configuration is of lower energy throughout the segregation profile than the '(b)' and '(d)' configurations. The configurational preference occurs because the '(a)' and '(c)' configurations lie underneath a surface oxygen, while the '(b)' and '(d)' configurations lie underneath a surface vacancy.

It should also be noted that the (100) segregation energies are substantially more negative than for the previous two surfaces. Nevertheless, E_S^{Ba} is again more negative than E_S^{Sr}, reflecting the difference in size of these ions.

6. Conclusions

Table 3 summarizes the calculated energies of segregation, E_S, for each cation to each surface considered in this work. This makes clear the dramatically different values for divalent compared to tetravalent species. In particular, Ce^{4+} and Zr^{4+} only segregate to the (100) surface while Ba^{2+} and Sr^{2+} segregate readily to all three surfaces. Furthermore, even for the (100) surface, E_S for Ba^{2+} and Sr^{2+} is much greater than for Ce^{4+} or Zr^{4+}. The greater driving force for divalent ion segregation is compounded by the greater depth at which the surface driving force becomes apparent. However, for the divalent dopants, E_S is also a strong function of defect cluster configuration with respect to the surface. Consequently, there is a cluster orientation preference towards surfaces which in a real system translates to configurational restrictions for the defects.

Overall, these results suggest that the release of fission products from grains of UO_2 in nuclear fuel will not be isotropic. In a real material, the distribution of surface types will clearly influence fission product release. This is important since fission product release is a limiting factor in fuel performance. Furthermore, surface structure will change due to grain growth *in situ* as a function of burn-up. However, this study shows how data may be generated from which mechanistic models predicting release of fission products can be developed.

Although definitive experimental data are not available, qualitative comparison can be made to the work of Sato *et al* [42], in which the behaviour of Ba and Zr in polycrystalline fuel specimens irradiated to burn-ups of 13.3 at.% was investigated. Using x-ray micro-scanning and x-ray micro-analysis to determine radial distributions of Ba and Zr, it was found that Ba concentrations increased in the radial direction, while Zr concentration remained homogeneous in the radial direction. This observation suggested to the authors that Ba easily migrates, while

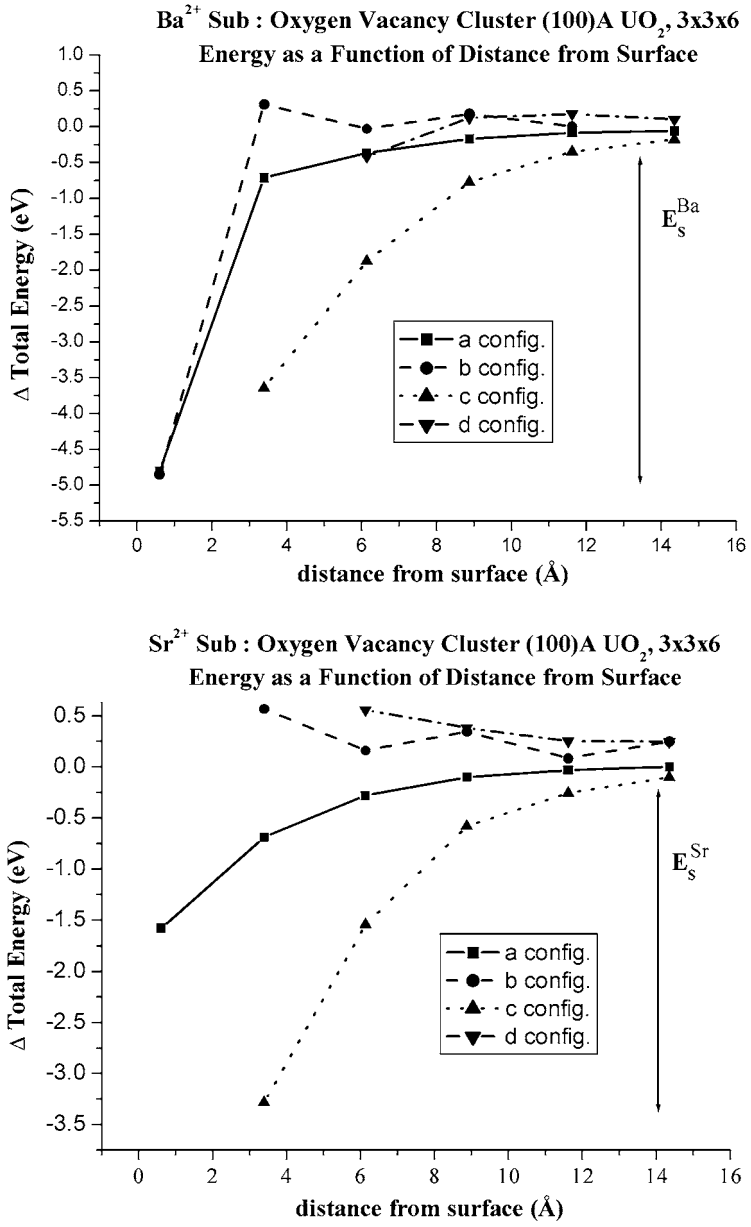

Figure 9. The calculated relative energies of the $\{(Ba_U/Sr_U)'':(V_O)^{\cdot\cdot}\}^x$ defect cluster as a function of depth from the (100)A surface, where E_S is the segregation energy.

Zr remains trapped in the fuel [42]. If UO_2 crystallites are dominated by (111) type low energy surfaces, the positive energy of segregation to this surface calculated for Zr is consistent with the observation.

Finally, we return to the work of Abramowski *et al* in which the morphology of UO_2 was predicted to be dominated by (111) surfaces, but by (100) surfaces in the presence of hydroxyl ions. In a similar manner, Ba and Sr may stabilize the (100) surface, thus influencing the morphology. Work is currently being carried out to elucidate this phenomenon.

Acknowledgment

This report and the work it describes were funded by the United Kingdom Health and Safety Executive. Its contents, including any opinions and/or conclusions expressed, are those of the authors alone and do not necessarily reflect HSE policy.

References

[1] Gibbs J W 1928 *The Collected Works of J Willard Gibbs* (New York: Longmans)
[2] Kleykamp H 1985 *J. Nucl. Mater.* **131** 221
[3] Grimes R W and Catlow C R A 1991 *Phil. Trans. R. Soc.* A **335** 609
[4] McCune R C and Wynblatt P 1983 *J. Am. Ceram. Soc.* **66** 111
[5] Roshko A and Kingery W D 1985 Segregation at special boundaries in MgO *J. Am. Ceram. Soc.* **68** C331
[6] Mukhopadhyay S M, Jardine A P, Blakely J M and Baik S 1988 Segregation of magnesium and calcium to the $(10\bar{1}0)$ prismatic surface of magnesium-implanted sapphire *J. Am. Ceram. Soc.* **71** 358–62
[7] Baik S and White C L 1987 *J. Am. Ceram. Soc.* **70** 682
[8] Baik S, Fowler D E, Blakely J M and Raj R 1985 Segregation of Mg to the (0001) surface of doped sapphire *J. Am. Ceram. Soc.* **68** 281–6
[9] Marcus H L and Fine M E 1973 *J. Am. Ceram. Soc.* **55** 568
[10] Lidiard A B and Norgett M J 1972 *Computational Solid State Physics* (New York: Plenum)
[11] Jackson R A, Catlow C R A and Murray A D 1987 *J. Chem. Soc. Faraday Trans.* II **83** 1171
[12] Jackson R A, Murray A D, Harding J H and Catlow C R A 1986 *Phil. Mag.* A **53** 27
[13] Grimes R W, Catlow C R A and Stoneham A M 1989 *J. Am. Ceram. Soc.* **72** 1856
[14] Olander D R 1976 *Technical Report* Tid-26711-p1, US Department of Commerce
[15] Colburn E A, Mackrodt W C and Tasker P W 1983 *J. Mater. Sci.* **18** 1917
[16] Duffy D M, Hoare J P and Tasker P W 1984 *J. Phys. C: Solid State Phys.* **17** L195
[17] Duffy D M and Tasker P W 1984 *Phil. Mag.* A **50** 143
[18] Tasker P W, Colburn E A and Mackrodt W C 1985 *J. Am. Ceram. Soc.* **68** 74
[19] Tasker P W and Mackrodt W C 1989 *J. Am. Ceram. Soc.* **72** 1576
[20] Davies M J, Kenway P R, Lawrence P J, Parker S C, Mackrodt W C and Tasker P W 1989 *J. Chem. Soc. Faraday Trans.* II **85** 555
[21] Kenway P R, Oliver P M, Parker S C, Sayle D C, Sayle T X T and Titiloye J O 1992 *Mol. Simul.* **9** 83
[22] Cooke D J and Parker S C 2002 *Geochim. Cosmochim. Acta* **66** A150
[23] Lawrence P J, Parker S C and Tasker P W 1988 *J. Am. Ceram. Soc.* **71** C389
[24] Sayle T X T, Parker S C and Catlow C R A 1994 *J. Phys. Chem.* **98** 13625
[25] Slater B, Catlow C R A, Gay D H, Williams D E and Dusastre V 1999 *J. Phys. Chem.* B **103** 10644
[26] Mackrodt W C 1987 *Mater. Sci. Res.* **21** 271
[27] LeSar R, Najafabadi R and Srolovitz D J 1989 *Phys. Rev. Lett.* **63** 624
[28] Najafabadi R, Wang H Y, Srolovitz D J and LeSar R 1991 *Acta Metall.* **39** 3071
[29] Battaile C C, Najafabadi R and Srolovitz D J 1995 *J. Am. Ceram. Soc.* **78** 3915
[30] Tasker P W 1979 *J. Phys. C: Solid State Phys.* **12** 4977
[31] Abramowski M 2001 Atomistic simulations of the uranium/oxygen system *PhD Thesis* Imperial College
[32] Vyas S, Grimes R W, Bulatov V and Abramowski M 2001 *Mol. Simul.* **26** 307–21
[33] Stanek C R 2003 Atomic scale disorder in fluorite and fluorite related oxides *PhD Thesis* Imperial College
[34] Mott N F and Littleton M J 1938 Conduction in polar crystals. I. Electrolytic conduction in solid salts *Trans. Faraday Soc.* **34** 485–99
[35] Born M 1923 *Atomtheorie des Festen Zustandes* (Leipzig: Teubner)
[36] Buckingham R A 1938 *Proc. R. Soc.* A **168** 264
[37] Dick B G and Overhauser A W 1958 Theory of dielectric constants of alkali halide crystals *Phys. Rev.* **112** 90–103
[38] Leslie M 1982 *Technical Report* Dl/sci/tm31t, SERC Daresbury Laboratory
[39] Gay D H and Rohl A L 1995 *J. Chem. Faraday Trans.* **91** 925
[40] Stanek C R, Grimes R W and Bradford M 2001 Segregation of fission products to surfaces of UO_2 *Mater. Res. Symp. Proc.* **654** AA3.32.1
[41] Shannon R D 1976 Revised effective ionic radii and systematic studies of interatomic distances in halides and chalcogenides *Acta Crystallogr.* A **32** 751–67
[42] Sato I, Furuya H, Arima T, Idemitsu K and Yamamoto K 1999 *J. Nucl. Sci. Technol.* **36** 775

[43] Grimes R W 1994 Solution of MgO, CaO and TiO_2 in α-Al_2O_3 *J. Am. Ceram. Soc.* **77** 378–84
[44] Zacate M O, Minervini L, Bradfield D J, Grimes R W and Sickafus K E 2000 *Solid State Ion.* **128** 243
[45] Vyas S, Grimes R W, Gay D H and Rohl A L 1998 *J. Chem. Soc. Faraday Trans.* **94** 427
[46] Grimes R W and Busker G 1996 *Nucl. Energy* **35** 403
[47] Busker G, Chroneos A and Grimes R W 1999 *J. Am. Ceram. Soc.* **82** 1553
[48] McCoy M A, Grimes R W and Lee W E 1997 *Phil. Mag.* A **75** 833